Modelling of Cu$_2$SnSeS chalcogenide quantum dots for optoelectronic applications

M. IRSHAD AHAMED[1,*], E. EDWARD ANAND[2], SAAHIRA AHAMED[3], N. PRATHAP[1]

[1]Department of Electronics and Communication Engineering, E.G.S. Pillay Engineering College, Nagapattinam – 611002, Tamilnadu, India
[2]Department of Science and Humanities, E.G.S. Pillay Engineering College, Nagapattinam – 611002, Tamilnadu, India
[3]Department of Computer Science, College of Computer Science and Information Technology, Jazan University, Jazan, Kingdom of Saudi Arabia

Material composition and size dependence are efficient techniques to regulate the absorption and emission of multiplex alloy quantum dots (QDs), similar to the size of binary and ternary QDs. Hence, in this communication we report for the first time, a model to investigate quaternary alloy Cu$_2$SnSeS to analyze the size and composition dependence of energy bandgap variation and wavelength by interpolation principles, Bohr and hyperbolic band model. The results underpin that the frequency of oscillation is inversely proportional to the energy bandgap and increases in copper proportion decrease the energy bandgap which offers plenty of opportunities to design for the application of various optoelectronic devices. Ultimately, these quaternary alloy QDs have been used as a source for fiber optic communication as a promising alternative to lead and cadmium-containing QDs.

1. Introduction

Telecommunication services nowadays are heavily reliant on optical fiber communication networks, which are required to handle high-speed, multi-channel, and long-distance transmission. Optical fiber communication efficiency doubles every 1.34 years, but the growth rate of silicon processors doubles every 2.2 years. These three operational wavelength ranges, 850 nm, 1310 nm, and 1550 nm, are extensively employed for data transmission in today's fiber optic communication systems [1]. The wavelength used for optical fiber communication, according to the International Telecommunication Union, Telecommunication Standardization Sector [ITU-T], corresponds to the wavelength band associated with the lowest transmission loss in the optical fiber [2], as illustrated in Fig. 1. The working wavelength range for telecommunications has been classified into six categories: O-band, E-band, S-band, C-band, L-band, and U/XL-band.

Because of its low attenuation loss in optical fibers, the C-band wavelength (1530-1565nm) gives the highest performance for long-distance communication of all three bands. Submarine optical transmission networks and many urban areas use it in conjunction with a wavelength division multiplexing (WDM) technology. By doubling the number of channels present in a single optical fiber, C-band boosts WDM transmission capabilities. Researchers are paying increasing attention to the development of a system to communicate ultra-long distances with a wavelength range of 1550 nm employing ternary or quaternary compound semiconductor lasers in recent generation fiber optic communication systems [3]. Fiber-optic communication and free-space optical communication (FSOC) use tunable transmitters like light-emitting diodes (LEDs) and laser diodes (LDs) to select the precise wavelength for data transmission.
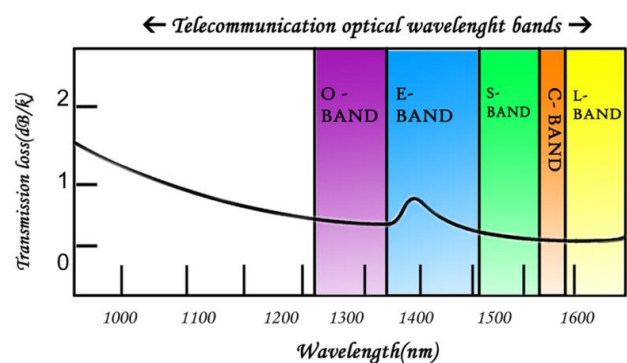
Fig. 1. Optical fiber transmission loss [2] (color online)

Traditional alloys have been employed to build innovative materials with increased structural, electrical, thermal, and mechanical properties for several decades, resulting in the development of high-performance materials that cannot be achieved by individual components. However, researchers have recently become interested in alloys to create new types of advanced nanosize materials (also known as nanoclusters or nanoparticles), which can have idiosyncratic properties that differ significantly from those of individual molecules and atoms or bulk solids [4-6].The fact that physical and chemical properties can be modified by modifying the size and composition of the clusters [7] is one of the main reasons for their interest in nanosize alloy materials.

Furthermore, because of their wide range of potential applications in sensors [8, 9], optics [10], biomedical engineering [11], electronics [12], and other fields, researchers and manufacturers are increasingly interested in metal-based nanosized semiconductor nanocrystals, commonly referred to as QDs.

Because of their tunable optical properties (i.e., energy bandgap) by varying the size and chemical composition of the material, QD-based metal chalcogenide alloys, mostly a group of II-VI and IV-VI semiconductors such as CdS, CdSe, CdS_xSe_{1-x}, PbS, PbSe, PbSeS semiconductor compounds are currently under extensive study in several research sectors such as QD laser diodes[13-15].Because, in addition to their sizes and forms, quaternary alloyed QDs' energy bandgap engineering can be accomplished by altering their composition. As a result, their optical properties may be designed and tuned, which is not possible with binary QDs. This can be accomplished by combining four different semiconducting semiconductors with different energy bandgaps, whereas an increase in the concentration of a major constituent element in the alloy or an increase in the concentration of a wide energy bandgap semiconductor usually results in a decrease in energy bandgap [16, 17].

Quaternary compounds offer greater flexibility to tune energy bandgap without relying on toxic elements such as indium and cadmium. Compounds consisting of two Group VI elements (e.g. Cu_2SnSeS) or two Group III elements (e.g. CIGaS) are referred to here as "pseudo-quaternary" systems. Ternary semiconductors are formed in such a way that cations or anions are substituted with ions of the same oxidation state. Ternary I–III–VI$_2$ semiconductors can conceptually be derived from binary II-VI semiconductors by replacing two divalent cations with one monovalent and one trivalent cation, whereas quaternary I–II–(VI,VI`)$_2$ compounds can be derived from ternary I–II-VI semiconductors by substituting two trivalent cations to one divalent and one tetravalent cation. Their main advantage is that they have no indium and its natural resources are prognosticated to become scarce in the future [18].

The number of component elements in optoelectronic semiconductors has steadily increased over the last 80 years, beginning with silicon in the 1950s and progressing to GaAs, InAs, and Cd (S, Se, and Te) in the 1960s, CuInSe$_2$ in the 1970s, Cu(In, Ga)Se2 in the 1980s, and Cu$_2$ZnSn(S, Se)4 and Ch3NH3PbI3 more recently. The properties of Cu$_2$ZnSnS4, Cu$_2$ZnSnSe$_4$, and their alloy Cu$_2$ZnSn(S, Se, &Te)$_4$ can be tuned more easily than in binary IV-VI or III-V semiconductors as the number of elements increases. The crystal structures of the I-IV-VI, I-II-IV-VI, and I-III-V semiconductors reveal chemical trends in their electronic band structure, allowing these semiconductors' band structure engineering. The energy bandgap of I-II-IV-VI compounds can be tuned from negative (conductor or topological insulator) to more than 4 eV. (Wide-gap semiconductor). Furthermore, due to the increased structural freedom, Cu$_2$ZnSn(S, Se & Te)4 and Cu$_2$Zn(Sn,Ge)Se4 alloys can tune their band gaps continuously and linearly based on their compositions. Because of the increased structural and chemical freedom of two-dimensional materials Cu$_2$ZnSn(S, Se, and Te)$_4$, point defects in the lattice are more likely, affecting optical and electrical properties and limiting performance in optoelectronic applications [19].

Djinkwi Wanda investigated variations in absorption layer thickness, absorption holes, and defect densities in Cu$_2$ZnSnS$_4$-based solar cells using the SCAPS-1D programme. They discovered the following based on their findings:

- The electrical parameters are significantly affected by an increase in absorber thickness.
- As the density of holes increases, so does the open-circuit voltage and fill factor.
- The flaws have a negative impact on performance parameters [20].

Uduakobong investigated the Brus model and discovered two distinct semiconductor QDs made of III-V and II-VI elements. Size dependence was observed using the particle in a box model, as predicted by the effective mass approximation method. The confinement energy and QD radius had an inverse relationship. PbS QDs from the III-V group have greater confinement than those from the II-VI group. The electron confinement in QDs was found to increase as the size of the dots decreased. There was a strong relationship between QD tunability and exciton Bohr radius. The replacement of continuum in the valence and conduction bands observed in the case of discrete atomic like energy levels as particle size showed a decreasing trend for adding value to QD materials. As a result, the model considering QD size with dependence on confinement energy agrees well with experimental observations [21].

Zoubeida et al. investigated the energy bandgap for ternary semiconductor QDs $Cd_{1-x}Zn_xS$ as a function of QD radius. The compositional dependencies are based on the assumption that both holes and electrons are confined in nanoranges and have an infinite potential barrier at the boundary level, but the excitonic binding energy is taken into account. The experimental data are in good agreement with the results, according to the results. This research has a lot of potential in a variety of technological applications, especially in the design and fabrication of optoelectronic devices based on IV-VI semiconductor QDs [22].

Ho et al. provided a review of Cu$_2$SnS$_3$ ternary nanostructures prepared via spray pyrolysis, Successive Ionic Layer Adsorption and Reaction (SILAR), and pulsed laser deposition. The bandgap energy was discovered to be between 0.98 and 1.87 eV. Good stability optoelectronic devices, particularly solar cells, were developed as a result of the energy bandgap values. The conversion efficiency of solar cells ranged between 0.11% and 0.84%. As demonstrated in this review, nanostructures can be controlled in a variety of ways to achieve desired applications [23].

Ming et al. investigated the structural, electronic, and optical properties of $GaAs_{1-x-y}Bi_xN_y$ alloy using first-principles calculations. HSE06 contains a more detailed description of the alloy (Hybrid Functional Calculation).

The band gap is effectively reduced by incorporating two elements into GaAs and distorting its lattice. A calculation of the alloy's optical properties revealed significant changes caused by the defect atom, which can be used to improve the alloy's performance in the future for long-wavelength applications [24].

For both types of quaternary alloys, the weighted-sum expression of quaternary parameter estimations via balancing surface bowing estimation errors is shown to be effective. Mei discovered $A_xB_{1-x}C_yD_{1-y}$ and $A_xB_yC_zD$. Weighted-sum schemes are better approximations to fundamental estimation than fundamental estimation. Using the correction terms, explicit molar fraction expressions of energy bandgap for AlGaInAs, AlGaInP, InAsPSb, GaInAsP, and GaInAsSb can be obtained with a deviation of less than 20 meV from the linear model (LM) polynomial expressions for LM compositions [25].

According to Kamalanathan et al. different phases of Cu_2SnS_3 nanoparticles with sizes ranging from 3nm to 37nm were observed in solution; ethylene glycol was used to avoid secondary phases. With bandgaps of 1.43 eV, 1.48 eV, and 1.64 eV, this material demonstrated good absorption properties in the UV to visible range. Cu_2SnS_3 materials can absorb a large amount of photocurrent as measured by photoconductivity. According to the findings of electronic and optical studies, Cu_2SnS_3 appears to be an ideal material for producing low-cost optical devices [26].

At the moment, obtaining the most reliable values of material parameters from the literature reported for a number of interesting semiconductor properties of quaternary systems is quite difficult. Sadao Adachi presented models for calculating various device parameters in compound alloys using the quaternary lattices AlGaAsSb, GaInAsSb, and InPAsSb, such as the lattice constant, bandgap energy, and refractive index. A number of optoelectronic-device applications are also thoroughly discussed using quaternary material parameters [27].

Compared to bulk materials, quaternary semiconductor nanocrystals offer several unique advantages [28]:

➢ Energy bandgap and electronic energy levels can be tuned by changing the size.

➢ The composition and internal structure are precisely controlled before materials processing.

➢ They can be deposited in various substrates by low-cost solution-based methods.

➢ Quaternary-alloyed QDs have a significantly long fluorescence lifetime of > 100 ns and excellent photostability.

➢ Quaternary-alloyed QDs exhibit unique composition-based optical properties, i.e., we can control the optical properties of QDs by adjusting the composition of the reactants.

By changing the composition of the quaternary alloys, each of the energy bandgap and lattice constant can be adjusted independently to achieve $Cu_2SnSeS/SnSeS$ structures with very low lattice-mismatch. Moreover, Cu_2SnSeS has not been studied in detail to date.

It must be demonstrated that modelling a solid semiconductor solution is a difficult undertaking in both computational and theoretical forms. Although first-principles computations can provide a physical understanding of alloy characteristics and compositional trends, they are generally impractical for experimenters [29]. To quickly evaluate the property of a given alloy, the experimenter commonly employs versions of Vegard's law principles. The tiny variation was effectively applied to the nonlinear variation of ternary alloy's energy bandgaps by Thomson et al. [30]. It consists of adding a quadratic term to the linear Vegard's law equation. Glisson et al. later offered expanded empirical interpolation on quaternary alloys. If no other acceptable representation is available, this method takes into account a weighted sum of four probable ternary alloys for determining energy bandgap analyses [31].

The quantum confinement effect is used to determine the energy bandgap and exciton Bohr radius of the quaternary alloy to investigate the size dependency. Quantum confinement is the effect of restricting electron movement in a zero-dimensional environment. As a result, energy states are discretized, giving birth to energy levels rather than energy band structure. Cu_2SnSeS QDs were used in this study to investigate variations in energy bandgap, wavelength, and exciton Bohr radius. This study could aid further analysis for researchers working on quaternary alloys and justify specific alterations in additives in alloys.

2. Theoretical framework

Energy bandgap plays a vital role in analyzing the property of semiconductors to determine their conductivity and wavelength. The optical and electronic properties of Cu_2SnSeS quaternary alloy will be investigated via the hyperbolic band model and Vegard's interpolation principle.

2.1. Energy band gap variation of Cu₂SnSeS by Vegard's Law analysis

The energy bandgap parameters of I-IV-VI₂ compound alloys, as well as their dependence on alloy, are critical device parameters that have previously attracted a lot of attention. However, the examination of key device parameters has been hampered by a lack of precise information on several material factors. This necessitates the use of some sort of interpolation scheme. Though experimental validation of Vegard's interpolation approach is still pending, it has the potential to give more valuable and consistent material properties across a wider variety of alloy compositions.

The empirical Vegard's law interpolation concept states that one of the important properties of an alloy, such as the energy bandgap, may be computed using a linear combination of those of the parent components. The ternary alloy energies are used to describe the non-linear relationship between transition energy and alloy

composition. The energy bandgap of the quaternary alloy (Cu_2SnSeS) for the alloy composition is calculated using Vegard's interpolation approach [32].

For Cu_2SnSeS quaternary alloy, the energy bandgap is calculated by following equation 1 [33-35]

$$E_g(x,y) = \frac{x(1-x)[y\,E_gCu_2S_nS_e(x)+(1-y)E_gCu_2S_nS(x)]}{x(1-x)+y(1-y)} + \frac{y(1-y)[xE_gCu_2S_eS(y)+(1-x)E_gS_nS_eS(x)]}{x(1-x)+y(1-y)} \quad (1)$$

where, $E_g(Cu_2SnSe)$, $E_g(Cu_2SnS)$, $E_g(Cu_2SeS)$, and $E_g(SnSeS)$ are represented as ternary alloy energy bandgaps. Most common for quaternary systems (x = 0,..., 1, y = 0,..., 1) with well-studied material properties. Four binary alloys (for x and y = 0 or 1) and four ternary alloys (for x or y = 0 or 1) are included in the compositional plane (x, y) of those quaternaries. Because the properties of materials vary significantly with their composition (x, y), interpolation schemes based on measured data of binary and ternary compounds have been developed [36].

2.2. Wavelength analysis by hyperbolic band model

The simple approximation method relates the radius of the nanomaterial and wavelength is the hyperbolic band model. The size-dependent Coulomb interaction of the Schrodinger equation for the excited state crystallite does not contribute significantly to subatomic particles [37]. As a consequence, the hyperbolic band model, where the effective mass of the electron (me*) inside the semiconductor and the effective mass of hole (mh*) outside the semiconductor [38]. Ignoring the Coulomb modifications of the overall energy bandgap shift, the

following equation may be derived for the size-dependent energy bandgap is given by

$$E_g(QD) = \sqrt{Eg^2 + \frac{\pi^2 2\hbar^2}{m0R^2}\frac{1}{2}\left(\frac{1}{me^*}+\frac{1}{mh^*}\right)} \quad (2)$$

as same as in the Brus model E_g (QD) and E_g are energy bandgap of semiconductor nanomaterial and bulk crystal respectively.

2.3. Variation of exciton Bohr radius

In General, an electron-hole pair in semiconductors created by the absorption of a photon is known as an exciton. The distance between the hole and the electron within an exciton is known as the Bohr radius of the exciton or exciton Bohr radius. The unique way to observe the quantum confinement effect in a semiconductor is by reducing the size of the material to below the exciton Bohr radius. Exciton Bohr radius (rB) of such bound electron-hole pair is given by [38]

$$r_{B=}\frac{\varepsilon\hbar^2}{4\pi e^2}\left(\frac{1}{me^*}+\frac{1}{mh^*}\right) \quad (3)$$

This rB signifies the characteristic length scale for the observation of quantum confinement effects in nanomaterials. The three cases to observe the quantum confinement effects are strong confinement, weak confinement, and moderate confinement.

3. Theoretical parameters

The following parameters which are substantial in theoretical calculations are listed in Table 1.

Table 1. Parameters of different elements.

S.No	Parameters	Values	Literature
1	Energy gap value of (Cu_2SnS_3)	0.9-1.5 eV	[39]
2	Energy gap value of (Cu_2SnSe)	0.8-1.1 eV	[40]
3	Energy gap value of (SnSSe)	1.7 eV	[41]
4	Energy gap value of (Cu_2SeS)	1.2-2 eV	[42]
5	The effective mass of electron and hole (Cu_2Se)	1.0 mo and 0.5 mo	[43]
6	Effective mass of electron and hole (Cu_2S)	0.3 mo and 0.8 mo	[44]
7	The effective mass of electron and hole (SnSe)	0.41 mo and 0.48 mo	[45, 46]
8	The effective mass of electron and hole (SnS)	0.35 mo and 0.55 mo	[46]
9	High frequency dielectric constant	~3.3	[47]

4. Results and discussion

The quaternary alloy's composition-dependent energy bandgap is estimated as a function of a generic compositional characteristic. This value is produced from a linear relationship between the compositions of groups IV (x) and VI (1-x), which is necessary for lattice matching. Equation 1 expresses the energy bandgap variation of Cu₂SnSeS using MATLAB. By altering the mole percentage of Cu, we first explore the probable energy bandgap of Cu₂SnSeS QDs. As may be seen in fig. 1, this is the case. By adjusting x=0.05, it may be tweaked from 0.99eV for x=0.1 to 0.67eV for x=1.0. If the mole fraction of Cu is increased; the energy bandgap of Cu₂SnSeSwill tend to be decreased due to the lower energy bandgap of Cu₂S₃and SnSe.
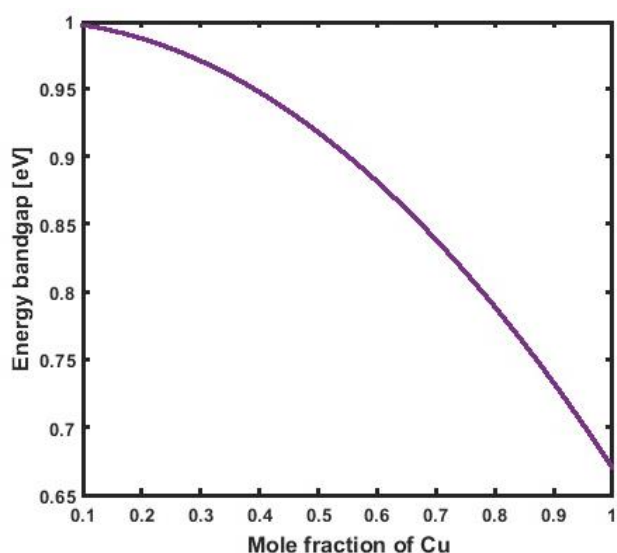
Fig. 2. Energy bandgap variation of Cu₂SnSeS (color online)
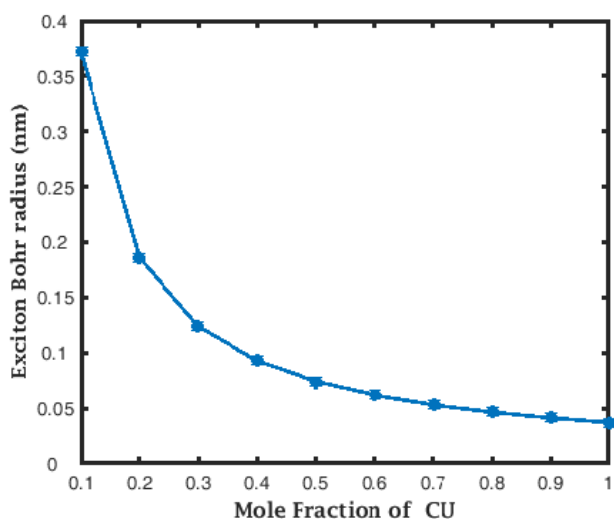
Fig. 3. Exciton Bohr radius variation (color online)

When the copper composition increases, the top of the valence band at Γpoint shifts up and the energy bandgap lowers. The energy bandgap of the material matches the

wavelength of LEDs and laser diodes. As a result, Cu₂SnSeSbased optoelectronic devices such as wavelength converters, sensors, and solar cells are seeing new applications.

Since quantum confinement effects are highly related to Bohr radius, it is important to calculate the exciton Bohr radius of Cu₂SnSeS QDs. As the Cu₂SnSeS has a direct band-gap at Γ-point viz., it is well known that quantum confinement affects the optoelectronic properties of nanoparticles with dimensions of several to dozens of nanometers. This results in asymmetrical broadening of line shapes compared to bulk particles. It becomes more evident when the size of nanoparticles is around the Bohr radius.

By varying the mole fraction of Cu, it is found that there are minimum and maximum values of exciton Bohr radius of the compound. The results show that the mole fraction of Cu increases as the exciton Bohr radius decreases. Fig. 3 shows that for a lower mole fraction of x=0.1, the calculated exciton Bohr radius is 0.37 nm this is the highest value of this compound, for maximum mole fraction x=1, the calculated value is 0.04 nm. Exciton Bohr radius decreases due to the high concentration of copper in this compound and this material is subjected to weak confinement of electrons which is probable, because of exciton Bohr radius is lower than the diameter of QDs. The coulomb interaction is retained and the exciton is confined in the weak confinement case, which corresponds to a radius R greater than the Bohr radius. As a result, discrete sub-bands of excitons with low energies are formed. For red and blue-shifted QDs copper concentration need to be reduced to achieve strong confinement.
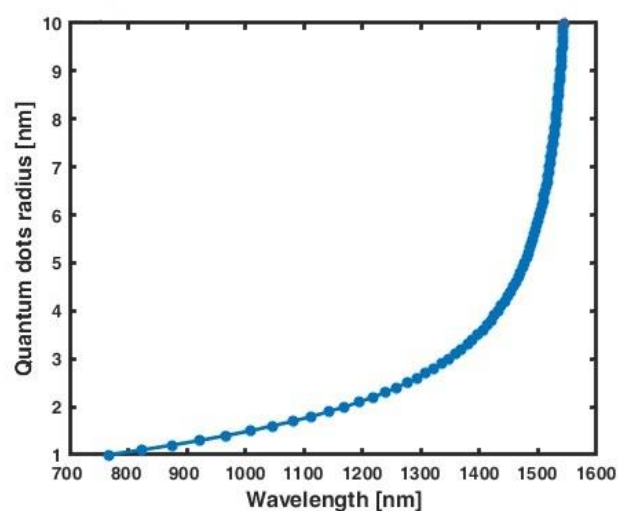
Fig. 4. Wavelength Vs. Quantum dots radius for Cu₂SnSeS QDs (color online)

Quaternary QDs can be tuned to specific incident energy levels based on material size owing to the quantum confinement effect. Furthermore, nanomaterial offers to increase the superior surface area that improves the absorption of properties per unit volume. Smaller QDs

have a higher energy bandgap and emit a short wavelength of light (blue shifted) and larger QDs have a lower energy bandgap and emit a longer wavelength (Red shifted).

Equation 3 was used to compute the wavelength of this quaternary compound Cu_2SnSeS. It has been discovered that by altering the size of QDs, a minimum and maximum wavelength value can be achieved. The ideal energy bandgap may be adjusted by changing the size of QDs, which aids in the discovery of various wavelength absorption ranges that cover visible to infrared. The absorption wavelengths vary from 769 nm to 1550 nm for Cu_2SnSeS, radius 'R' with values ranging from 1 nm to 10 nm, which includes the visible and infrared regions.

The wavelength spectra tested at different QD sizes are shown in Fig. 4. The radius of a quantum dot is 1 nanometer, and the absorption wavelength is 769 nm, which is close to visible spectra. The absorption wavelength in the near-infrared range is somewhat increased when the radius of QDs is slightly raised from 2 nm to 3 nm (1168 nm to 1348 nm).

It has been proposed that a new type of optical fiber cable be developed in order to lower the cost and improve performance. Fiber optic sources, which are fabricated with tunable wavelength light emitting devices, are being used in this type of application as previously stated. Tunability of wavelength was an expensive feature of earlier fiber optic systems. It is now possible to develop QDs technology using ternary and quaternary semiconductor materials.

LDs and LEDs are key sources of input for fiber optic communication, as they offer input for the fiber to convey a signal from one location to another. The three most widely used operating wavelength ranges are 850 nm, 1310 nm, and 1550 nm. For long-distance communication, 1550 nm (C-band) is the best option. We can easily attain this wavelength with Cu_2SnSeS QDs, and it has been observed that it can be set to 1310 nm at a 2.74 nm radius. As a result, it's a great wavelength for making LEDs and LDs for fiber optic communication in the C- and O-band ranges. Cu_2SnSeS QDs would be able to utilize the near-infrared and infrared ranges for solar cell applications, increasing the efficiency of the solar cell by forming more electron-hole pairs.

To the best of our knowledge, there is no theoretical simulation based on the hyperbolic band model and Vegard's law and no experimental values of the optoelectronic properties of Cu_2SnSeS alloy. Therefore, our calculations can be used to cover the data deficit for the studied alloy. The work in reference [48] presents many similarities in the objectives and methodologies of the present work. In both cases, the quaternary and ternary alloys were studied using the exciton Bohr principles and the Brus/Hyperbolic band model. On the other hand, Vegard's law was used to calculate the optoelectronic properties. In this work, an improved interpolation principle is used to calculate the energy bandgap variation. Globally, the quaternary alloys studied in both works exhibit the same behavior. Our results and reference [48] are consistent with each other, especially the similarities in

energy gap $Eg(x)$ and wavelength. There is a decrease in energy bandgaps in quaternary alloy Cu_2SnSeS compare to ternary alloy Cu_2SnS_3 pointing to weak interactions between elemental constituents (alloying interaction effect) and an increase in dielectric constant with a higher alloy composition. This energy difference is somewhat smaller than corresponding value of ~0.9 eV for when comparing their group-VI anion atoms (Se). This changes may help to fine tune optical properties of this alloy for fiber optic communication and solar cell applications. The stoichiometric tunability of Cu-based QDs is high. Furthermore, altering or adding the composition, in addition to changing the sample size, is another effective method of tuning the emission of QDs. By altering the ratio of precursors used in certain reactions, this can be achieved. It is generally observed that when group VI elements is incorporated into Cu-based ternary systems, the absorption and emission spectra are blue shifted [49]. Finally, the results of the present study confirm that Cu_2SnSeS quaternary alloys are a suitable material for the fabrication of near-infrared and infrared light-emitting and detecting devices as reported in reference [48].

5. Conclusion

The wavelength, energy bandgap, and exciton Bohr radius of Cu_2SnSeS QDs have all been effectively modelled. The energy bandgap variation for Cu_2SnSeS quaternary alloy on the copper concentration x ($0.1 \leq x \leq 1.0$) is seen to be almost linear. Furthermore,Cu_2SnSeS quaternary alloys show strong absorption in the wavelength range (769-1550 nm) corresponding to the energy bandgap range from 1.6eV to 0.8eV.The acquired results regarding the studied properties of the Cu_2SnSeS quaternary alloy are found to be a potential semiconductor material for the manufacture of stable optoelectronic devices, particularly LEDs and LDs for fiber optic communication sources, Solar cells, both single and multiple junction solar cells, can benefit from this material. The main findings of this study point to the significant use of these materials in telecommunications, such as WDM devices. These findings are useful in the creation of novel materials and in determining the energy bandgap with limited data.

References

[1] E. Agrell, M. Karlsson, A. Chraplyvy, D. Richardson, P. Krummrich, P. Winzer, K. Roberts, J. Fischer, S. Savory, B. Eggleton, M. Secondini, F. Kschischang, A. Lord, J. Prat, I. Tomkos, J. Bowers, S. Srinivasan, M. Brandt-Pearce, N. Gisin, Journal of Optics **18**, 063002 (2016).

[2] M. Irshad Ahamed, K. Sathish Kumar, Materials Science-Poland **37**, 225 (2019).

[3] Y. Tamura, H. Sakuma, K. Morita, M. Suzuki, Y. Yamamoto, K. Shimada, Y. Honma, K. Sohma, T. Fujii, T. Hasegawa, Optical Fiber Communication

Conference Post deadline Papers, OSA Technical Digest (online) (Optical Society of America, 2017), paper Th5D.1.

[4] L. An, Y. Yu, X. Li, W. Liu, H. Yang, D. Wu, S. Yang, Materials Research Bulletin **49**, 285 (2014).

[5] M. Farle, Nature **542**, 35 (2017).

[6] R. Ferrando, J. Jellinek, R. Johnston, Chemical Reviews **108**, 845 (2008).

[7] Z. Qin, F. Zhang, Applied Surface Science **285**, 912 (2013).

[8] Michal Borecki, Piotr Doroz, Przemyslaw Prus, Pawel Pszczólkowski, Jan Szmidt, Korwin-Pawlowski, Jaroslaw Frydrych, Andrzej Kociubinski, Mariusz Duk, Int. J. Adv. Syst. Meas. **7**, 57 (2014).

[9] M. Borecki, M. Geca, M. Duk, M. L. Korwinpawlowski, J. Electron. Commun. Eng. Res. **2**, 1 (2017).

[10] S. Subramanian, S. Ganapathy, M. Rajaram, A. Ayyaswamy, Materials Chemistry and Physics **249**, 123127 (2020).

[11] L. Wang, D. Xu, J. Gao, X. Chen, Y. Duo, H. Zhang, Science China Materials **63**, 1631 (2020).

[12] L. Xu, S. Yuan, H. Zeng, J. Song, Materials Today Nano **6**, 100036 (2019).

[13] M. Landry, T. Morrell, T. Karagounis, C. Hsia, C. Wang, Journal of Chemical Education **91**, 274 (2013).

[14] D. Zhou, M. Lin, Z. Chen, H. Sun, H. Zhang, H. Sun, B. Yang, Chemistry of Materials **23**, 4857 (2011).

[15] Sashchiuk, D. Yanover, A. Rubin-Brusilovski, G. Maikov, R. Čapek, R. Vaxenburg, J. Tilchin, G. Zaiats, E. Lifshitz, Nanoscale **5**, 7724 (2013).

[16] M. Regulacio, M. Han, Accounts of Chemical Research **43**, 621 (2010).

[17] O. Adegoke, T. Nyokong, P. Forbes, Journal of Alloys and Compounds **645**, 443 (2015).

[18] Dmitry Aldakov, Aurelie Lefrançois, Peter Reiss, Journal of Materials Chemistry C **1**, 3756 (2013).

[19] Dingrong Liu, Dan Han, Menglin Huang, Xian Zhang, Tao Zhang, Chen Min, Shiyou Chen, Chinese Physics B **27**(1), 018806 (2018).

[20] M. Djinkwi Wanda, S. Ouédraogo, F. Tchoffo, F. Zougmoré, J. M. B. Ndjaka, International Journal of Photoenergy **2016**, 2152018 (2016).

[21] S. Uduakobong, Journal of Physics **3**, 28 (2017).

[22] K. Zoubeida, S. Nabil, D. Mohamed, International Journal of Applied Chemistry **12**, 573 (2016).

[23] S. Ho, S. Gincy, A. V. Sharadrao, Journal of Engineering and Applied Sciences **13**, 4152 (2018).

[24] Ming Su, Chong Li, Pengfei Yuan, Fengfei Rao, Yu Jia, Fei Wang, Optics Express **22**, 30633 (2014).

[25] T. Mei, Journal of Applied Physics **101**, 013520 (2007).

[26] M. Kamalanathan, H. Shamima, R. Gopalakrishnan, K. Vishista, Mat. Technol. **33**, 72 (2017).

[27] Sadao Adachi, Journal of Applied Physics **61**, 4869 (1987).

[28] G. Donati, R. Kaspi, K. Malloy, Journal of Applied Physics **94**, 5814 (2003).

[29] A. Thompson, J. Woolley, Canadian Journal of Physics **45**, 255 (1967).

[30] C.Williams, T. Glisson, J. Hauser, M. Littlejohn, Journal of Electronic Materials **7**, 639 (1978).

[31] Liu Chao, Wei Zhi-Peng, An Ning, He Bin-Tai, Liu Peng-Cheng, Liu Guo-Jun, Acta Physica Sinica **63**, 248102 (2014).

[32] Y. Wang, A. Suna, W. Mahler, R. Kasowski, Journal of Chemical Physics **87**, 7315 (1987).

[33] V. Swaminathan, A. Macrander, "Materials aspects of GaAs and InP based structures" Prentice Hall Publisher, New Jersey, 108 (1991).

[34] G. String, Journal of Electronic Materials **10**, 919 (1981).

[35] R. Moon, G. Antypas, L. James, Journal of Electronic Materials **3**, 635 (1974).

[36] M. Guden, J. Piprek, Modelling Simulation of Material Science Engineering **4**, 349 (1996).

[37] K. Nanda, F. Kruis, H. Fissan, S. Behera, Journal of Applied Physics **95**, 5035 (2004).

[38] M. I. Ahamed, K. S. Kumar, E. E. Anand, A. Sivaranjani, J. Ovonic. Res. **16**, 245 (2020).

[39] M. I. Ahamed, M. Ahamed, A. Sivaranjani, S. Chockalingam, Chalcogenide Letters **18**, 245 (2021).

[40] M. Norako, M. Greaney, R. Brutchey, Journal of the American Chemical Society **134**(1), 23 (2011).

[41] H. Im, Y. Myung, Y. Cho, C. Kim, H. Kim, S. Back, C. Jung, D. Jang, Y. Lim, J. Park, J. Ahn, RSC Advances **3**(26), 10349 (2013).

[42] A. Sharma, M. Yewale, G. Chavan, D. Kambale, S. Potdar, Materials Science **33**(2), 397 (2015).

[43] N. Khusayfan, H. Khanfar, Results in Physics **12**, 645 (2019).

[44] P. Lukashev, W. Lambrecht, T. Kotani, M. van Schilfgaarde, Physical Review B **76**, 195202 (2007).

[45] N. Koteeswara Reddy, M. Devika, E. Gopal, Solid State and Materials Sciences **40**, 359 (2015).

[46] V. Deb, V. Kumar, Physica Status Solidi B **254**, 1600379 (2016).

[47] S. Tripathy, A. Pattanaik, Optical Materials **53**, 123 (2016).

[48] M. I. Ahamed, K. S. Kumar, Materials Science – Poland **37**, 108 (2019).

[49] Xue Bai, Finn Purcell-Milton, Yuri K. Gunko, Nanomaterials **9**, 85 (2019).

_____

*Corresponding author: irshad_bcet@yahoo.co.in